铸铁表面激光熔凝行为及温度场数值模拟

伊 鹏， 刘衍聪， 石永军， 姜 浩
（中国石油大学(华东) 机电工程学院，东营 257061）

摘 要：为明确铸铁表面激光熔凝过程的热响应规律，考虑随温度变化的材料热物性参数和相变潜热影响，建立铸铁表面激光动态熔凝的三维数值模型并进行了验证，预测值与试验值吻合良好，采用该模型分析了热响应温度场规律及不同工艺参数的映射关系. 结果表明，铸铁表面激光熔凝较钢材可获得更大的熔透深度，熔池内、外形成较大温度梯度且分别以深、宽方向分量为主，降低扫描速度和减小光斑尺寸可以获得更大的温度梯度；熔池尺寸随扫描速度和光斑半径的增大而减小，提高激光扫描速度并减小光斑尺寸可以增大凝固相变速度.

关键词：激光熔凝；铸铁；数值模拟；瞬态温度场；熔池
中图分类号：TG174；TN249 文献标识码：A 文章编号：0253－360X(2011)08－0081－04

伊 鹏

0 序 言

在石油、石化和航天造船等领域，机械装备种类繁多，部分装备如箱体等的工况条件恶劣，造成大量设备过早发生失效破坏，由于激光具有良好的聚焦特性，能量高度集中，加工时间短、热影响区小，可得到更细小的重熔组织，保证材料力学性能的同时减小热变形.

激光热修复涉及复杂的物理、化学冶金变化，其中表面熔凝(LSM)是重要过程，对该过程的热响应研究是进一步明确基体重熔区(RMZ)和热影响区(HAZ)组织变化的基础. 目前在材料微观形态及力学性能方面的试验研究较为充分[1－3]，田宗军、席明哲等人[4,5]对45钢激光重熔温度场进行了研究；沈以赴、陈泽民等人[6,7]分别对45钢和Q235钢激光熔覆温度场进行了研究；石永军等人[8,9]研究了激光热成形钢板温度变形场相似性及温度梯度机制. 以上研究通过数值模拟建立可靠模型，对材料表面激光热作用的温度场规律进行描述并取得了一定成果，而铸铁作为机械装备的常用材料研究较缺乏[10,11]. 因此为进一步明确铸铁表面的激光熔凝温度场及熔池行为规律，文中采用有限元法建立灰铸HT200表面激光熔凝过程模型，预测温度场分布，为进一步研究高性能的铸铁表面改性层提供理论依据.

收稿日期：2010－08－30
基金项目：山东省自然科学基金资助项目(Y2007F76)；新疆克拉玛依市科技基金资助项目(SK2008－52)；中国石油大学(华东)创新基金资助项目(BZ1008)

1 激光熔凝物理模型

激光熔凝过程物理模型如图1所示，为提高计算效率对模型进行一定的简化，假设环境状态稳定，忽略材料的熔融流动作用，认为材料各向同性，热物性参数仅与温度有关.

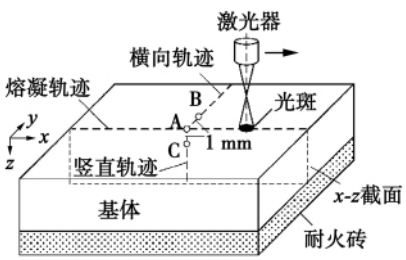

图1 激光熔凝模型
Fig. 1 Schematic of LSM

热传导是主要的热传递方式，与环境的对流和辐射是主要热损失方式，激光能量以高斯分布热流密度的形式加载，表达式为

$$q=\frac{2PA}{\pi R^2}e^{\left(-\frac{2r^2}{R^2}\right)} \tag{1}$$

式中：P 为激光输出功率；R 为能量密度减小到光斑中心能量密度的 $1/e^2$ 时的光束半径；r 为考察点至光束中心的距离；A 为材料表面激光能量吸收率.

考虑铸铁材料片状石墨大幅提高对激光能量的吸收率(约 60% ~80%),因此对其修正取 $A=0.75$.

数值模型中采用第二和第三类边界条件,分别为热流输入和对流换热输出. 试件初始温度为环境温度 20 ℃,基体下表面与耐火砖接触设为绝热,激光热流密度载荷施加于上表面光斑区域,图 1 中各区域热边界条件如表 1 所示.

表 1 热边界条件

Table 1 Thermal boundary conditions

施加区域	边界条件
上表面	$\Gamma_1+\Gamma_2+\Gamma_3$
下表面	$q=0, h=0, \varepsilon=0$
侧面	$\Gamma_2+\Gamma_3$

采用内插和外推法确定不同温度下材料的热物性参数. 选择八节点热耦合单元 Solid70 对求解区域进行有限元离散,为保证求解精度和效率激光扫描路径附近采用较精细网格划分,其它区域则划分为较大单元,单元总数为 11 700.

2 熔凝过程数值模拟

2.1 数值模型的试验验证

线切割法制备尺寸为 25 mm × 20 mm × 8 mm 的 HT200 铸铁试样,采用连续 CO_2 激光器,初选加工参数为 $P=1\ 000$ W,扫描速度 $v=1.2$ m/min 和光斑半径 $r=1$ mm,观察熔池边界,试验值与计算值对比如图 2 所示.

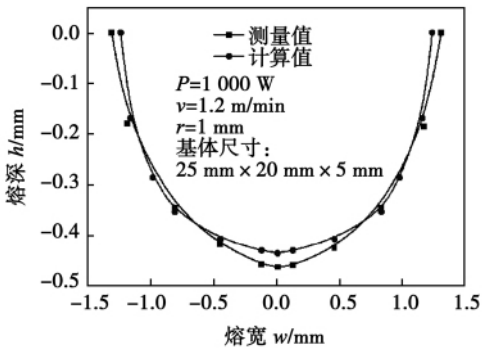

图 2 熔池边界计算值与试验值对比

Fig. 2 Comparison between calculated and measured results of molten pool boundary

实际硬化区和熔化区深度比计算值稍大,最大误差比例小于 9%,误差主要原因是建模时热源模型的简化以及材料参数的插值等,总体来说吻合较好,因此由该模型得出的计算结果是可靠的.

2.2 熔凝热循环

激光表面熔凝 0.1,0.6,1.25 s 时铸铁试样温度分布如图 3 所示,随高能激光束的快速移动,光斑附近区域温度分布相对稳定,受辐照材料迅速熔融并凝固,在试样表面造成巨大的温度梯度和冷却速度.

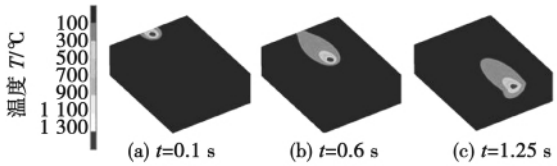

图 3 激光熔凝过程温度场分布

Fig. 3 Temperature distributions in process of LSM

2.3 温度场的影响分析

不同扫描速度 v 和光斑半径 r 情况下,熔池温度最高点所在截面沿 y,z 向温度及其梯度分布如图 4,图 5 所示. 由温度分布的总体规律可知,温度梯度在 y 方向变化剧烈并在熔池边界处存在拐点,而在 z 向则为单减变化,且在熔池以内温度梯度以 z 向分量为主. 较大的温度梯度驱动熔池快速对流,

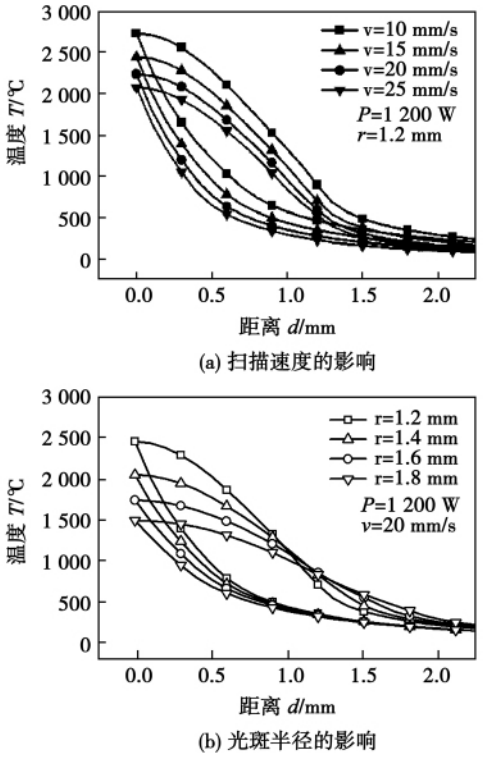

图 4 不同工艺参数时的熔池截面温度分布

Fig. 4 Temperature distributions on molten pool section with different parameters

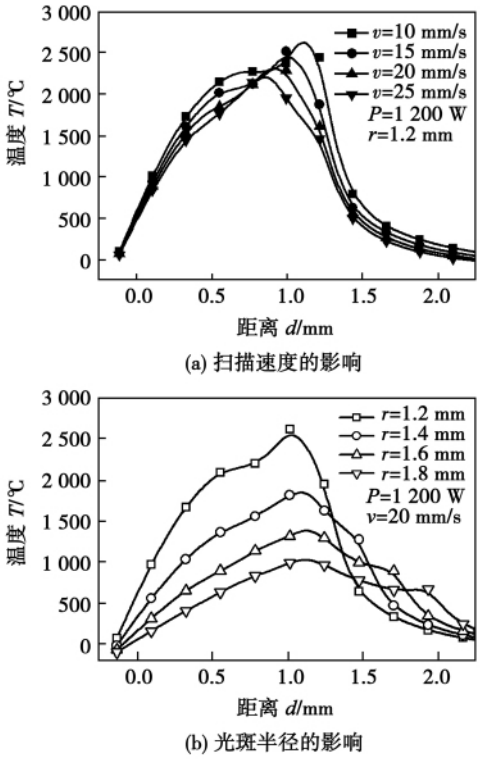

图 5　不同工艺参数时的熔池表面温度梯度分布

Fig. 5　Temperature gradient distributions in pool section with different parameters

熔池以外温度梯度以 y 向为主,熔池内流速度则以 z 向为主,可知热流方向较单一.

由图 4a 可知,熔池截面温度分布受激光扫描速度 v 的影响较小,各位置温度值变化一致,随 v 的增大熔池尺寸有所减小,而图 4b 中光斑半径 r 的变化在熔池内影响较大,距熔池中心越远受影响越小,在 y 向距离 1.2 mm 处则基本不受影响,而熔池之外的温度变化情况与前述规律相反,因此增大光斑半径缩小了材料重熔区但增大了热影响区域.

温度梯度分布如图 5 所示,由图 5a 可知在熔池边界附近区域温度梯度随 v 的增大而降低,v 增大一倍时 y 向的熔池边界处最大降低了 22%,而熔池以内基本未受影响; 图 5b 中可以看出 r 的变化对梯度分布影响较大,r 增大 33% 时 y 向梯度最大降低 54%. 因此降低扫描速度和减小光斑尺寸均可以获得更大的温度梯度,但影响区域不同,前者在熔池边界附近有作用但影响较弱,后者则在熔池内重熔区有显著影响,因此可更有效的增大熔凝过程温度梯度.

2.4　熔凝行为的影响分析

不同扫描速度 v 和光斑半径 r 条件下沿扫描方向的 x-y,x-z 面熔池边界如图 6 所示,最大熔池长度约 1.8 mm,最大熔宽 2.1 mm,熔深 0.5 mm 分别出现于熔池长度的 1.0 mm 和 1.2 mm 处,熔池在宽度方向的发展较深度方向滞后; 凝固部分熔池边界的法向为凝固速度方向,y 向边界曲率较大,最大熔宽处凝固方向垂直于扫描方向,在尾部偏离. 因此可以推知,熔池中的冷却散热及结晶潜热通过液相散失的方向不一致,晶体生长不能保持稳定,各方向凝固速度的共同作用导致主晶轴上易长出二,三次晶轴并形成树枝晶; 而在 z 向,凝固方向较统一,基本垂直于扫描方向,有利于生成取向一致、挺直的定向柱晶.

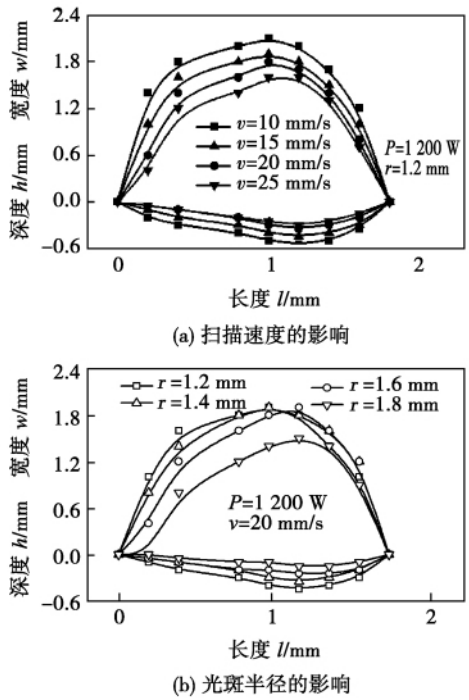

图 6　不同工艺参数时的熔池边界

Fig. 6　Comparison of molten pool boundary with different parameters

由图 6a 可知,随扫描速度的增大,熔宽、熔深均减小,深度方向边界受影响较大达 44%,但当 v 增至 20 mm/s 时熔深减小为 0.3 mm 并且不随 v 变化; 同时随扫描速度的增大,熔池凝固边界的法向逐渐垂直于扫描方向,因此新生成的枝晶也趋向于该方向生长; 图 6b 中随光斑半径 r 的增大,熔池尺寸亦呈减小趋势,熔深受影响较明显,在 r 增至 1.8 mm 时熔深减小为 0.2 mm,另外熔池凝固边界的法向基本不受影响,因此表层组织的生长和取向主要受控于激光扫描速度.

3　结　　论

(1) 基体表面的凝固速度方向不一致; 熔池内

的温度分布受光斑半径的影响大，增大光斑半径缩小重熔区但扩大热影响区，降低扫描速度和减小光斑尺寸均可以获得更大的温度梯度.

(2) 熔池内、外温度梯度分别以深度、宽度分量为主，热流方向单一，其边界在熔宽方向的移动滞后于熔深方向，熔池尺寸随扫描速度和光斑半径的增大而减小.

参考文献:

[1] 雷剑波，杨洗陈，陈 娟，等. 激光熔覆熔池表面温度场分布的检测[J]. 中国激光，2008，35(10)：1605－1608.
Lei Jianbo，Yang Xichen，Chen Juan，*et al*. Measurement of surface temperature field distribution in molten pool of laser cladding [J]. Chinese Journal of Lasers，2008，35(10)：1605－1608.

[2] 李明喜，修俊杰，赵庆宇，等. 钼对钴基合金激光熔覆层组织与耐磨性的影响[J]. 焊接学报，2009，11(4)：17－21.
Li Mingxiu，Xiu Junjie，Zhao Qingyu，*et al*. Effect of Mo content on microstructure and wear resistance of Co-based coatings by laser cladding [J]. Transactions of the China Welding Institution，2009，11(4)：17－21.

[3] 杨尚磊，张文红，李法兵，等. 纳米Y_2O_3-Co基合金激光熔覆复合涂层的分析[J]. 焊接学报，2009，30(2)：79－83.
Yang Shanglei，Zhang Wenhong，Li Fabing，*et al*. Investigation on laser cladded nano-Y_2O_3 and cobalt based composite coating [J]. Transactions of the China Welding Institution，2009，30(2)：79－83.

[4] 田宗军，王东生，黄因慧，等. 45钢表面激光重熔温度场数值模拟[J]. 材料热处理学报，2008，29(6)：173－178.
Tian Zongjun，Wang Dongsheng，Hang Yinhui，*et al*. Numerical simulation of temperature field of laser remelting on 45 steel [J]. Transactions of Materials and Heat Treatment，2008，29(6)：173－178.

[5] 席明哲，虞 钢. 连续移动三维瞬态激光熔池温度场数值模拟[J]. 中国激光，2004，31(12)：1527－1532.
Xi Mingzhe，Yu Gang. Numerical simulation for the transient temperature field of 3D moving laser molten pool [J]. Chinese Journal of Lasers，2004，31(12)：1527－1532.

[6] 沈以赴，顾冬冬，李守卫，等. 多组元金属粉末选区激光烧结三维瞬态温度场模拟[J]. 南京航空航天大学学报，2008，40(5)：611－616.
Shen Yifu，Gu Dongdong，Li Shouwei，*et al*. Simulation of 3-D transient temperature field during selective laser sintering of multi-component metal powder [J]. Journal of Nanjing University of Aeronautics & Astronautics，2008，40(5)：611－616.

[7] 陈泽民，曾 凯，廖丕博，等. 激光熔覆模压预置层的温度场模拟与参数预测[J]. 材料热处理学报，2009，30(1)：188－191.
Chen Zemin，Zeng Kai，Liao Peibo，*et al*. Simulation on temperature field of pre-coated layer formed by steel dieing and parameters predicting in Laser cladding [J]. Transactions of Materials and Heat Treatment，2009，30(1)：188－191.

[8] 石永军，沈 洪，姚振强，等. 激光热成形温度场和变形场相似性研究[J]. 光电子·激光，2006，17(8)：1019－1024.
Shi Yongjun，Shen Hong，Yao Zhenqiang，*et al*. Similarity of temperature and deformation fields in the laser forming [J]. Journal of Optoelectronics. laser，2006，17(8)：1019－1024.

[9] Shi Y J，Yao Z Q，Liu F，*et al*. Temperature gradient mechanism in laser forming of thin plates [J]. Optics & Laser Technogogy，2007，39(4)：858－863.

[10] 储 训，马援东. 铸铁铸钢激光表面改性材料及工艺研究[J]. 农业工程学报，2001，17(4)：22－25.
Chu Xun，Ma Yuandong. Material and technology research on surface of cast iron and cast steel by laser cladding [J]. Transactions of The Chinese Society of Agricultural Engineering，2001，17(4)：22－25.

[11] 李 风，王大承，张永俊. HT300孕育铸铁激光表面改性研究[J]. 应用激光，2005，25(5)：303－305.
Li Feng，Wang Dacheng，Zhang Yongjun. Study on the laser surface strength of inoculated cast iron HT300 [J]. Applied Laser，2005，25(5)：303－305.

作者简介: 伊 鹏，男，1983年出生，博士研究生. 主要从事机械装备激光修复方面的科研工作. 发表论文7篇. Email: yipupc@163.com

通讯作者: 刘衍聪，男，教授，博士生导师. Email: liuyc@upc.edu.cn

welding process and welding stirring pin shape are the key of high-quality fillet welding joint. When the rotation speed is 30 – 40 rad/s and the welding speed is 90 – 120 mm/min, we can get a high-quality weld appearances.

Key words: friction stir welding; outer fillet welding; 2519 aluminum alloys

Ultra-high cycle fatigue behaviors of Q345 bridge steel welded joint FANG Donghui[1], LIU Yongjie[2], CHEN Yiyan[3], WANG Qingyuan[2] (1. Department of Civil Engineering & Architecture, College of Jincheng, Sichuan University, Chengdu 610065, China; 2. Department of Mechanics and Engineering Science, Sichuan University, Chengdu 610065, China; 3. Shenzhen Municipal Design & Research Institute, Shenzhen 518029, China). p 77 – 80

Abstract: The high cycle and ultra-high cycle fatigue properties of Q345qC base metal and circular butt weld joint were studied by using the ultrasonic fatigue testing technique. The experimental results show that during $10^5 - 10^9$ cycles, the fatigue strength of welded joint is much less than that of base metal, and both their S-N curves descend continuously. Fracture can still occur on base metal beyond 10^7 cycles and on welded steel beyond 5×10^6 cycles. The observation of fracture surface shows cracks mainly initiate from welded toes at fusion area or geometric discontinuity at the surface in welded steel. Furthermore, fatigue failure occurs at the geometric discontinuity area in the high stress regime but occurs at welded toes in the low stress regime.

Key words: ultra-high cycle fatigue; welded joint; ultrasonic fatigue test; S-N curve; fracture surface

Numerical simulation of dynamic laser melting behavior and temperature field on cast iron surface YI Peng, LIU Yancong, SHI Yongjun, JIANG Hao (College of Mechanical and Electronic Engineering, China University of Petroleum, Dongying 257061, China). p 81 – 84

Abstract: For explicitly understanding the thermo-mechanism of laser melting process on cast iron, a validated dynamic three-dimensional numerical modal for this process was established by taking into account the thermal physical parameters and latent heat of the material. The temperature field and the relationships between different process parameters were studied with this model, and the simulation results were in accordance with the experimental results. The results indicate that the penetration depth of the laser melting process on cast iron is grater than that on the steel. The large temperature gradients inside and outside the molten pool are dominated by the depth and width components respectively. A larger temperature gradient is gained through reducing scan speed and spot size. The pool is shrunk by the increase of scan speed and spot radius; the solidification speed is raised with the increase of laser scan speed and reduction of the spot size.

Key words: laser melting process; cast iron; numerical simulation; transient temperature field; molten pool

Microstructure and properties of Er-containing aluminum alloy TIG weld joints JIN Likun[1], LI Xiaoyan[1], HE Dingyong[1], JIANG Jianmin[1], YANG Dongxia[2], NIE Zuoren[2] (1. College of Materials Science and Engineering, Beijing University of Technology, China; 2. New Functional Materials Key Laboratory of Ministry of Education, Beijing University of Technology, Beijing 100124, China). p 85 – 88

Abstract: To study the strengthening effect and mechanism of Er element on the weld, the remelting welding of Al-Mg alloy with Er was adopted, and the organizational structure and mechanical properties of the joint were observed. The results show that there is primary Al_3Er phase precipitation on the grain boundaries in weld, but the quantity of it is fewer than that of in the base material, and the precipitation doesn't form a continuous ring. The secondary Al_3Er precipitation also can be found in the welding, but the precipitation phase quantity is very few. Er elements will presence in the solid solution or segregation way. The strength of Er element on the weld joint is mainly based on the primary Al_3Er to refine the grain. The effect of the secondary phase on the weld joint is small, and so the weld joint mechanical properties decrease evidence. The tensile strength of welded joints is 297 MPa, and the strength coefficient of welded joints is 72% of base material. Tensile fracture position is mainly in the center of the weld and near the fusion zone.

Key words: primary phase; secondary phase; fine-grain strengthening; precipitation strengthening

Mathematical model based on MATLAB for intersection seam of sphere and tube ZHAO Jie[1,2], HU Shengsun[1,2], SHEN Junqi[1,2], CHEN Changliang[2], DING Wei[1] (1. Tianjin Key Laboratory of Advanced Joining Technology, Tianjin University, Tianjin 300072, China; 2. School of Materials Science and Engineering, Tianjin University, Tianjin 300072, China). p 89 – 92

Abstract: The welding process of complex space curve, such as intersection seam of sphere and tube, is difficult in the field of welding automation, and the construction of a mathematical model of intersection seam is a prerequisite for the welding process. After a mathematical model of intersection curve of sphere and tube is established with MATLAB software, by further analysis, the intersection curve can be simplified to plane curve. By considering the thickness effects of the sphere, some amendments to the model of J-shaped groove weld are made by increasing $\triangle D$ and $\triangle d$ two corrections in the diameter directions of sphere and tube respectively. All functions such as graphics and output data, are integrated into a GUI (Graphics User Interface) based on MATLAB programming, and the GUI is converted to a standalone application which is efficient and convenient, which provided a theoretical basis for robot welding and controlling of this seam weld.

Key words: welding automation; intersection curve of sphere and tube; mathematical model; graphics user interface

Influence of different cooling rates on microstructure of Ti-6Al-4V titanium alloy thermal simulation specimens WANG Jinlin[1], GAN Zhanghua[1], CHEN Yiming[1], XIAO Jianzhong[2] (1. College of Materials Science and Metallurgical Engineering, Wuhan University of Science and Technology, Wu-